

ARTICLE OPEN



A shift towards broader and less persistent Southern Hemisphere temperature anomalies

Itamar Karbi¹✉ and Rei Chemke¹

Temperature anomalies considerably influence the regional climate and weather of the extratropics. By the end of this century, climate models project an intensification of synoptic temperature variability in the Southern Hemisphere mid-latitudes. This intensification, however, comprises temperature anomalies with various length scales and periods, which might respond differently to anthropogenic emissions. Here, we find a shift, in coming decades, towards spatially larger and less persistent temperature anomalies in the Southern Hemisphere mid-latitudes. A shift towards larger length scales is also found during regional extreme heat events. The shift in length scale and duration is found to stem from changes in the meridional heat flux of atmospheric perturbations. Our results emphasize the importance of investigating the length scale and period-dependent changes in the mid-latitude climate, to prevent masking the different impacts of various length scales and periods, and thus provide more accurate climate projections for the mid-latitudes.

npj Climate and Atmospheric Science (2023)6:200; <https://doi.org/10.1038/s41612-023-00526-9>

INTRODUCTION

The weather and climate of the extratropics are largely affected by temperature anomalies. On daily to monthly time scales, temperature anomalies modulate synoptic weather (i.e., day-to-day variations), and they also account for extreme heat and cold events. On multi-decadal time scales, synoptic temperature variability largely affects the distribution of heat and moisture across the extratropics¹. Given their crucial role in setting the weather and climate of the mid-latitudes, even modest changes in temperature anomalies would have large climatic^{2–5} and societal impacts⁶.

By the end of the century, synoptic temperature variability in the Southern Hemisphere (SH) mid-latitudes is projected to considerably intensify during both summer and winter, and shift poleward during summer^{7–9} (Supplementary Fig. 1b, c). Given the turbulent nature of the mid-latitude flow, which results in non-uniform distribution of the intensity of mid-latitude phenomena across length scales and periods^{10–12}, the projected intensification in SH synoptic temperature variability might also be scale dependent; temperature anomalies of different length scales and periods may respond differently to anthropogenic forcings. For example, by the end of the century, while large atmospheric waves will become stronger (in terms of their kinetic energy, for example), small waves will become weaker^{13–17}. In terms of temperature anomalies, previous studies also found a length scale and period-dependent response to anthropogenic forcings, but mainly in the Northern Hemisphere (NH). The spatial scale of atmospheric waves was found to affect the occurrence of atmospheric and marine heatwaves^{18–21}. In addition, in both recent and coming decades, NH mid-latitude phenomena (e.g., temperature anomalies, heat flux and precipitation) were found to become more persistent^{22–25}.

In the SH, on the other hand, the projected changes in the persistence and size of temperature anomalies are more uncertain. For example, previous studies reached opposite conclusions regarding the future changes in the persistence of SH temperature anomalies; while some studies argued for an increase in the

persistence of SH temperature anomalies²³, others argued for a decrease in persistence²². The opposite findings might stem from examining different length scales and periods. Furthermore, these studies have not examined the full spectrum of length scales and periods, and have not accounted for the codependence of the period and length scale of the anomalies (the dispersion relation²⁶). To accurately assess how temperature anomalies will change in coming decades, without masking out the different impacts of the various length scales and periods, it is critical to investigate the future changes in temperature anomalies across all length scales and periods.

Lastly, temperature anomalies associated with extreme heat events (i.e., heatwaves and warm spells), both atmospheric and marine, are of particular interest due to their adverse weather impacts^{27,28}. Previous studies have identified that, globally, both atmospheric and marine heatwaves are projected to become more intense and frequent over the 21st century^{29–31}, and some trends are already detectable today^{32–36}. However, while the duration of future NH heatwaves over land is projected to increase^{29,37}, future changes in the duration of SH heatwaves over land are less pronounced^{29,38–40}. Moreover, there is large uncertainty regarding the projected changes in the length scale of extreme heat events in the SH.

RESULTS

Broader and less persistent temperature anomalies

To examine the length scale and period-dependent future changes in temperature anomalies, we conduct a two-dimensional Fourier analysis in longitude and time to the SH mid-latitude synoptic temperature variability over the 20th and 21st centuries (Methods). Unlike previous examples of scale-dependent Fourier analysis¹⁵, which focused on dynamical changes in atmospheric waves, here, we not only conduct a zonal and temporal Fourier analysis, but also we examine a near-surface thermodynamic quantity. Our analysis is thus mostly valid to the SH, since in the NH a near-surface Fourier transform is

¹Department of Earth and Planetary Sciences, Weizmann Institute of Science, Rehovot, Israel. ✉email: itamar.karbi@weizmann.ac.il

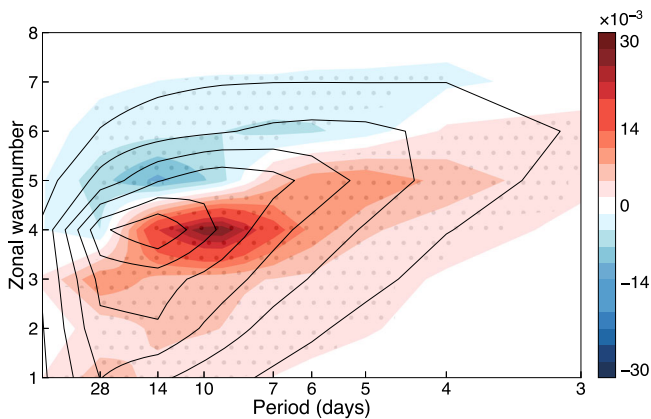


Fig. 1 Future spatially larger and less persistent temperature anomalies. The response of mid-latitude temperature variability (K^2) to anthropogenic emissions (difference between the 2080–2099 and 1980–1999 periods) in CMIP6 mean as a function of wavenumber and period. Black contours show the climatological spectrum of temperature variability (averaged over the 1980–1999 period). Gray dots show regions where at least 80% of the models agree on the sign of change.

limited due to topography⁴¹ (note the lack of a spectral shift and the disagreement across models in NH temperature variability spectral changes, Supplementary Fig. 2).

Prior to analyzing the future changes in temperature variability, we first note that previous studies found biases in the climatology and trends of SH mid-latitude dynamics in climate models^{42–44}. Here, on the other hand, CMIP6 adequately simulate both the historic climatology and trends in the temperature variability spectrum (Supplementary Figs. 3, 4); since the source of SH mid-latitude model bias (e.g., storm tracks) was argued to be related to upper-level dynamics⁴⁴, such model bias might have only a minor impact on near-surface variables. This gives us confidence in using CMIP6 models to assess the projected temperature variability changes.

We analyze the response of the temperature variability spectrum to anthropogenic emissions (difference between the 2080–2099 and 1980–1999 periods) in 21 models that participate in the Coupled Model Intercomparison Project Phase 6 (CMIP6) under the historical (through 2014) and the Shared Socio-economic Pathways 5–8.5 (through 2100) forcings (Methods)⁴⁵. We find that, by the end of this century, temperature anomalies are projected to become spatially larger and less persistent (shading in Fig. 1). While spatially small and long-lasting anomalies (top-left region in Fig. 1) will overall weaken by 4%, relative to the 1980–1999 period (blue colors in Fig. 1), and up to 30% in certain frequencies and wavenumbers, the spatially large and short-lived anomalies (bottom and bottom-right regions in Fig. 1) are projected to overall intensify by 9% (red colors in Fig. 1), and up to 60% in certain frequencies and wavenumbers.

To further quantify these spectral changes we next separately examine the changes in length scale and period. First, the length scale of temperature anomalies is projected to increase for all periods (Fig. 1); temperature variability at low wavenumbers is projected to strengthen, while at high wavenumbers to weaken. Quantitatively, relative to the 1980–1999 period, the increase in the weighted-mean wavelength (Methods) is up to 7% across all periods (i.e., a shift of 550 km in the mid-latitudes; Supplementary Fig. 5). Note that since at high latitudes the spectrum is concentrated more at low wavenumbers, it is conceivable that the reduction in wavenumber (i.e., the increase in length scale) is merely a manifestation of the poleward shift of temperature variability (Supplementary Fig. 1a)⁴⁶. However, we find that the increase in length scale occurs throughout the mid-latitudes

(Supplementary Fig. 6), confirming that it is not an artifact of the poleward shift of temperature variability.

Second, a shift towards less persistent anomalies is evident at wavenumbers 4 and above; while short-lived anomalies are projected to intensify, long-lasting anomalies are projected to weaken. At wavenumbers 3 and below, although temperature variability shows an intensification over all periods, most of the intensification occurs at periods shorter than the period of maximum temperature variability over the end of the 20th century, suggesting a shift towards less persistent anomalies for these wavenumbers as well (compare red colors and black contours in Fig. 1). Overall, the reduction in the weighted-mean period (Methods) is up to 11% across all wavenumbers (i.e., a shift of 0.8 days; Supplementary Fig. 5). The period dependent changes found here could explain the contradicting results of previous studies^{22,23}, of an increase and a decrease in the duration of temperature anomalies; analyzing only a limited part of the spectrum, and not accounting for the codependence of the length scales and periods, might lead to the opposite conclusions regarding the impacts of anthropogenic emissions on the period of temperature anomalies in the SH. In other words, a change in the persistence, for example, could be assessed only by examining the shift in period of the entire spectrum and not just the strengthening/weakening of the variability at a given period. In addition, not only that we find that the duration of temperature anomalies is projected to decrease, but also their overall phase speed (which accounts for both the mean and eddy phase speeds) is projected to increase, leading to less persistent temperature anomalies (Supplementary Fig. 7).

Lastly, ozone depletion and recovery were found to affect the large-scale atmospheric flow in the SH summer⁴⁷. It is thus conceivable that the projected spectral shift found here might also be driven by changes in ozone concentrations. However, not only the spectral shift is found in both summer and winter (Supplementary Fig. 8a, b), but also examining the spectral changes between the pre-ozone depletion and post-ozone recovery periods⁴⁸ (i.e., removing the ozone impacts) yields similar results (Supplementary Fig. 9). Thus, ozone is not likely the main anthropogenic forcing agent contributing to the future spectral changes in temperature anomalies in the SH.

Scale-dependent changes during extreme heat events

Are the above shifts in length scale of SH temperature anomalies also evident during extreme heat events? To answer this question, we next conduct a zonal Fourier analysis by pooling together days of regional extreme heat events (Methods). We here conduct only a zonal, and not a temporal, spectral analysis of extreme heat events since these events are not continuous in time.

Similar to the spectral shift found for all temperature anomalies (Fig. 1), we find that temperature anomalies are projected to become spatially larger also during extreme heat events (Fig. 2); the weighted-mean wavelength of temperature variability, averaged over the mid-latitudes, is projected to increase by 5% (with 95% confidence interval of 3–7%) during extreme heat events (compare gray lines in Fig. 2). Note that changes in the length scale of temperature anomalies during extreme heat events are not uniformly distributed across all latitudes. Over the equatorward part of the mid-latitudes, temperature anomalies of long wavelengths during extreme events are projected to strengthen, while short anomalies weaken. Over the poleward part of the mid-latitudes, while an intensification of temperature anomalies during extreme heat events is evident across all length scales, the maximum intensification occurs at length scales larger than the length scale of maximum temperature variability over the 1980–1999 period, resulting in the overall increase in scale by the end of the century.

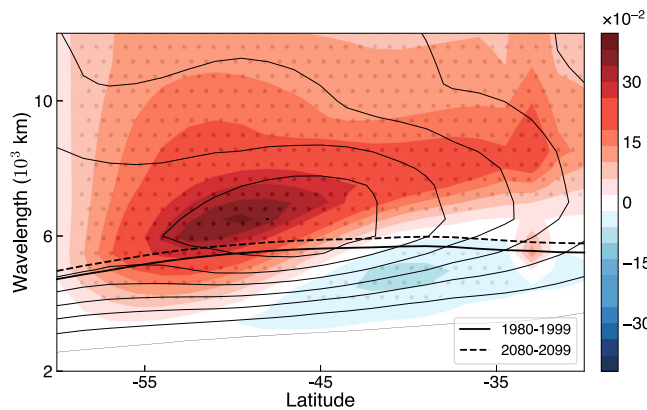


Fig. 2 Spectral changes in temperature variability during regional extreme heat events. The response of temperature variability (K^2) to anthropogenic emissions (difference between the 2080–2099 and 1980–1999 periods) in CMIP6 mean as a function of wavelength and latitude during regional extreme heat events (shading). Black contours show the climatological spectrum of temperature variability (averaged over the 1980–1999 period). Gray dots show regions where at least 80% of the models agree on the sign of change. The solid and dashed black lines show the weighted mean wavelength averaged over the 1980–1999 and 2080–2099 periods, respectively.

The source of the spectral shift in temperature anomalies

To elucidate the source of the shift towards larger and less persistent temperature anomalies, we examine in spectral space the different terms of the temperature variability tendency equation (Methods). In particular, temperature variability could be modified via four processes: zonal, meridional, and vertical advection (including adiabatic heating) of temperature variability, and diabatic heating.

For simplicity, to illustrate the impacts of the different terms, we investigate their contributions to the shift in wavenumber (Fig. 3a, c) and period (Fig. 3b, d), separately. Specifically, we examine the temperature variability equation at the wavenumber and period where the spectral shift is most clearly evident (i.e., at a period of 14 days and zonal wavenumber 5); similar results are found when examining the role of the different terms across the entire spectrum (Supplementary Fig. 10). We find that the term that mainly contributes to the increase in the length scale and the decrease in the persistence of temperature anomalies is the meridional advection of temperature variability (solid red lines in Fig. 3c, d). All other terms have minor and mitigating effects. The critical role of meridional advection in temperature variability changes is similar to its role in driving changes in the temperature distribution across the extra-tropics, as found in previous studies^{7,9,49–51}.

The meridional advection term can be decomposed into three different types of processes (Fig. 3c, d; Methods): (i) eddy-mean interactions, which account for the interactions between the zonal and time anomalies and the time-mean zonal-mean fields, (ii) eddy-eddy interactions, which account for the interactions between the zonal and time anomalies of different length scales and periods, and (iii) hybrid eddy-mean/eddy-eddy interactions which account for all interactions with either the zonal anomalies of the time mean field or the temporal anomalies of the zonal mean field. Examining the contribution of the different interaction terms reveals that the changes in eddy-mean interactions are the source of the shift towards spatially larger and less persistent temperature anomalies (dashed red lines); the other interactions have minor mitigating effects (dash-dotted red lines). Further decomposing the eddy-mean interactions (Supplementary Fig. 10g, h), we conclude that it is the interaction between the

meridional eddy heat flux and the zonal and monthly mean meridional temperature gradient that results in the projected spectral shift.

The interaction between the eddy heat flux and the meridional temperature gradient also plays a major role in the growth of atmospheric perturbations^{26,52} (i.e., storms, temperature anomalies, etc.), since it represents the extraction of available potential energy from the mean flow to the eddies⁵³. Thus, the spectral shift found here might be driven by processes that affect the growth of eddies, e.g., the vertical structure of the zonal mean zonal wind (the meridional temperature gradient), static stability, and tropopause height. We thus next conduct a linear normal mode instability analysis to the linearized quasi-geostrophic equations (similar to previous studies^{14,15,54}, only here for the SH), and examine the projected changes in the eddy growth rate using the mean fields (zonal wind, static stability, and tropopause height) as input parameters (Methods).

First, similar to the shift in length scale of temperature variability, we also find a shift of the eddy growth rate towards larger length scales (solid black line in Supplementary Fig. 11). Second, we find that changes in static stability and tropopause height contribute to the strengthening of large length scales and weakening of small length scales, while changes in the zonal wind contribute to strengthening of the growth rate over all length scales. Although the above growth rate analysis is only conducted as a function of length scale, similar results are found when linking the changes in the mean fields to the length scale and period-dependent eddy heat flux changes. Specifically, the increase in static stability and tropopause height are well correlated with the weakening of the eddy heat flux (averaged over regions of the spectrum with a projected weakening in eddy heat flux, Supplementary Fig. 12e, f). They are also correlated, though to a lesser extent, with the strengthening of the eddy heat flux (Supplementary Fig. 12b, c). The changes in the temperature gradient (i.e., wind shear), on the other hand, are only correlated with the strengthening of the eddy heat flux (Supplementary Fig. 12a, d).

DISCUSSION

The turbulent nature of the mid-latitude flow results in a non-uniform distribution of temperature variability across different length scales and periods. Since different physical processes control this distribution of temperature variability, temperature anomalies of different length scales and periods might respond differently to anthropogenic emissions. Thus, examining the future length scale and period-dependent temperature variability changes is crucial to avoid masking out their distinct future climate impacts.

However, to date, there is a large uncertainty in future length scale and period-dependent changes in temperature variability in the SH. Previous studies examined the changes in temperature variability over specific length scales or periods, and have not accounted for the codependence of the temporal and length scales of the anomalies, thus reaching opposite conclusions regarding future changes in temperature variability^{22,23}. Here we examine the future changes in SH near-surface synoptic temperature variability across a wide range of length scales and periods, and find that temperature anomalies will become broader and less persistent by the end of this century (similar results are evident throughout the troposphere; Supplementary Fig. 13). In other words, while the intensity of spatially large-scale and short-lived anomalies will increase, the intensity of spatially small-scale and long-lasting anomalies will decrease in coming decades. Thus, we expect that while the reduction in the persistence might reduce the impact of temperature anomalies, the increase in length scale is expected to increase their impact since it will affect wider areas.

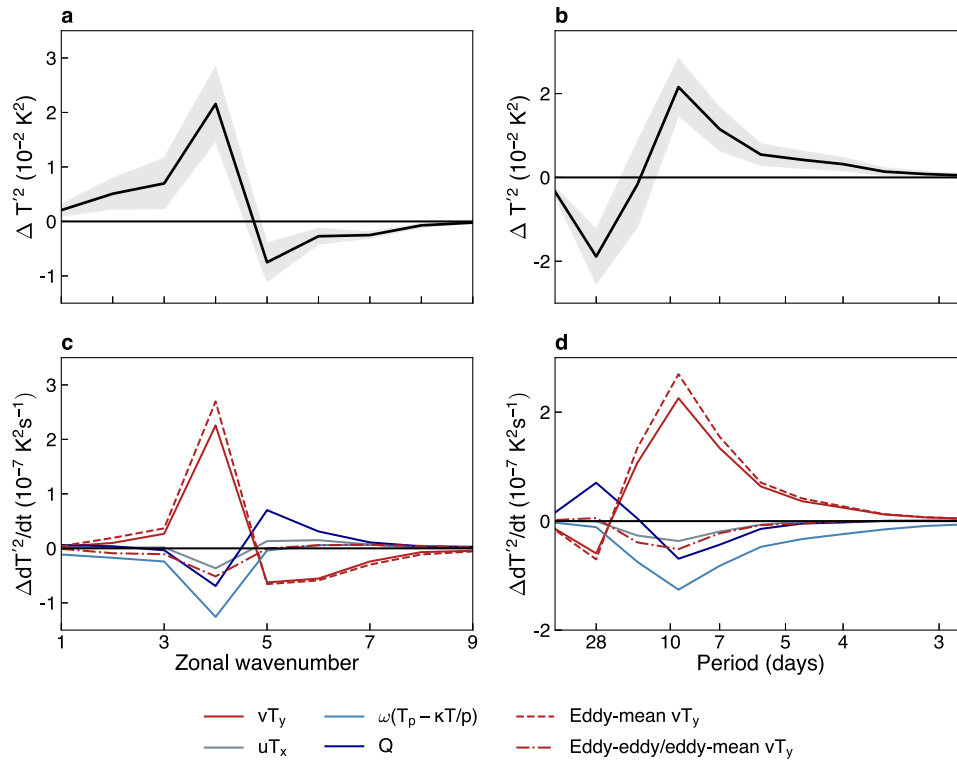


Fig. 3 Spectral changes in the temperature variability tendency equation. The response of temperature variability as a function of (a) zonal wavenumber (at a period of 14 days) and (b) period (at zonal wavenumber 5). Black solid lines show the CMIP6 mean and shading the 95% confidence interval based on a Student's t-distribution. c, d The contribution of each term in the temperature variability equation to the CMIP6 changes in temperature variability. Red, gray, light, and dark blue solid lines show the contribution of meridional, zonal, and vertical advection and diabatic heating terms, respectively. Dashed and dash-dotted lines show the contribution of the meridional advection term decomposed to eddy-mean/eddy-eddy and the sum of the eddy-eddy and the hybrid eddy-mean/eddy-eddy interactions, respectively.

The source of the projected shift of SH temperature anomalies to larger length scales and shorter periods is found to stem from a similar shift of the meridional heat flux by atmospheric perturbations. More specifically, changes in the vertical temperature structure are found to mostly contribute to this shift, emphasizing that eddy heat fluxes of different length scales and periods might have different sensitivities to changes in the vertical temperature profile. In contrast, in the NH, previous work argued for the impact of Arctic amplification, and the associated reduction in the meridional temperature gradient, in modulating the length scale and duration of NH mid-latitude phenomena^{55,56}. The different roles of the vertical and meridional temperature gradients could partly explain the hemispheric asymmetry in the length scale and period-dependent changes of mid-latitude phenomena by the end of this century (e.g., the increase vs. the decrease in persistence in the NH and SH, respectively).

Finally, our results also show that temperature anomalies during extreme heat events are also expected to increase in length scale and thus to affect wider areas. This adds to the projected increase in the intensity and frequency of such extreme events in the SH^{32–34}. Given the substantial climate impacts of temperature anomalies, our results highlight that for scientists to provide the most accurate projection of mid-latitude climate change, it is imperative to examine the changing mid-latitude climate as a function of length-scale and period.

METHODS

CMIP6

We use daily and monthly outputs of zonal and meridional winds, geopotential height, temperature and maximum surface

temperature from 21 models (we use all models with available data) that participate in the Coupled Model Intercomparison Project Phase 6⁴⁵ (CMIP6, Supplementary Table 1) and select only the “r1i1p1f1” member (in order to weigh all models equally) under the Historical (through 2014) and Shared Socioeconomic Pathways 8.5 (SSP5-8.5, through 2100) experiments.

Reanalyses

We use 6 hourly outputs of temperature from five different reanalyses: ERA5⁵⁷, NCEP2⁵⁸, JRA-55⁵⁹, MERRA2⁶⁰ and CFSv2⁶¹. Reanalyses provide the best estimate for the state of the atmosphere in recent decades, by constraining atmospheric models with observations (e.g., rawinsondes, satellite, and surface marine and land data), thus creating a continuous estimate of the atmospheric state in space and time.

Temperature variability

Synoptic temperature variability is defined as deviations from zonal and monthly mean temperature field. We calculate the synoptic temperature variability as a function of length scale and period by conducting a two-dimensional Fourier transform, in longitude and time, to the temperature field ($T'_{k,\omega}$, where subscripts k and ω represent the zonal and temporal Fourier components, and prime stands for the deviation from the monthly-mean zonal-mean field) and then multiply by its complex conjugate to obtain the temperature variability in spectral space ($T'^2_{k,\omega}$). To examine the temperature variability changes as a function of phase speed, we follow previous studies⁶², and transform $T'^2_{k,\omega}$ to $T'^2_{k,c}$ using the following relation $c = \omega(2\pi a \cos \phi)/k$, where c is the phase speed, a is Earth radius and ϕ is the latitude.

Specifically, at each latitude, the spectral analysis is performed at 850 mb over 28-day segments, and we average the spectrum over the mid-latitudes (30°S–60°S) and over the entire year. Following previous studies⁶³, we choose to analyze the 850 mb level as not only that it holds continuous spatial and temporal temperature data on an isobaric surface, which enables conducting the Fourier analysis, but it also allows us to assess the future climate impacts of temperature variability near the surface. Nevertheless, similar results are found throughout the troposphere (Supplementary Fig. 13). In addition, we analyze here the annual mean spectrum since similar behavior is evident in both winter and summer (Supplementary Fig. 8). Lastly, the weighted-mean wavenumber (k) is calculated, following previous studies¹³, as $\bar{k}(\omega) = \sum_k k |T'(k, \omega)|^2 / \sum_k |T'(k, \omega)|^2$. Similarly, the weighted-mean frequency (ω) is calculated as $\bar{\omega}(k) = \sum_\omega \omega |T'(k, \omega)|^2 / \sum_\omega |T'(k, \omega)|^2$.

Regional extreme heat events

The spectral analysis of regional extreme heat events is applied only for days that satisfy the CTX90pct definition⁶⁴, i.e., events of at least three consecutive days when the maximum daily temperature averaged over the SH climate regions (South Pacific, South Atlantic, South America, and Australia, Supplementary Fig. 1) is above the 90th percentile of either the 1980–1999 or the 2080–2099 periods (we pool together days of extreme events from each region). We note that the shift of temperature anomalies towards larger length scales is also evident when considering extreme events at each region separately (Supplementary Fig. 13), and when assessing extreme events using the SH mid-latitudes mean maximum daily temperature (Supplementary Fig. 14). Lastly, the shift to larger length scales is also evident when analyzing days that satisfy the CTN90pct criterion for a heatwave⁶⁴, i.e., events of at least three consecutive days when the minimum daily temperature averaged over the SH climate regions is above the 90th percentile (Supplementary Fig. 15).

Temperature variability tendency equation

To elucidate the mechanisms underlying the changes in the zonal and temporal spectra of temperature variability, we spectrally analyze the temperature variability tendency equation, which is derived by spectrally decomposing the temperature tendency equation and multiplying by the complex conjugate of the spectrally decomposed temperature field ($T'_{k,\omega}^*$),

$$\frac{1}{2} \frac{\partial |T'|^2}{\partial t} \Big|_{k,\omega} = \text{Re} \left(T'_{k,\omega}^* (-uT_x - vT_y - w(T_p - \kappa T/p) + Q) \Big|_{k,\omega} \right), \quad (1)$$

where u, v, w are the zonal, meridional, and vertical velocities, T_x, T_y, T_z are the zonal, meridional, and vertical temperature gradients respectively, $w\kappa T/p$ is adiabatic heating ($\kappa = R/c_p$, where R is the gas constant, which equals $287 \text{JK}^{-1}\text{kg}^{-1}$, and c_p is the specific heat capacity of air, which equals $1003 \text{JK}^{-1}\text{kg}^{-1}$), Q is diabatic heating, calculated as a residual, and asterisk denotes a complex conjugate.

We next decompose the temperature and meridional velocity in the meridional advection term in Eq. (1) as follows,

$$X = [\bar{X}] + [\tilde{X}] + \bar{X}' + X', \quad (2)$$

where over-bar and square brackets stand for zonal mean and monthly mean, respectively, and the tilde and dagger stand for deviations from the zonal mean and monthly mean, respectively. This yields a decomposition of the meridional advection term as follows,

$$T'(vT_y) = \text{NEM} + \text{LEE} + \text{HEM}, \quad (3)$$

where $\text{NEM} = T'(v'[\bar{T}_y] + [\tilde{v}]T'_y)$ represents the eddy-mean interactions between the eddy fields (deviations from both zonal and monthly means) and the time mean zonal mean fields, $\text{LEE} = T'v'T'_y$ represents the eddy-eddy interactions (interactions between eddies of different length-scales and periods), and $\text{HEM} = T'(v'[\tilde{T}_y] + [\tilde{v}]T'_y + v'\bar{T}_y + \tilde{v}'T'_y + \tilde{v}'[\tilde{T}_y] + [\tilde{v}]\bar{T}_y)$ represents the hybrid eddy-mean/eddy-eddy interactions, which account for all interactions with either the zonal anomalies of the time mean field or the time anomalies of the zonal mean field.

Linear normal mode instability analysis

To examine the future changes in the eddy growth rate, we follow previous studies^{14,15,54}, and conduct a linear normal mode instability analysis to the quasigeostrophic equations, linearized about a mean state,

$$\frac{\partial q'}{\partial t} + \bar{u} \frac{\partial q'}{\partial x} + \frac{\partial \psi'}{\partial x} \frac{\partial \bar{q}}{\partial y} = 0, \quad H_p < p < p_s,$$

$$\frac{\partial}{\partial t} \frac{\partial \psi'}{\partial p} + \bar{u} \frac{\partial}{\partial x} \frac{\partial \psi'}{\partial p} - \frac{\partial \psi'}{\partial x} \frac{\partial \bar{u}}{\partial p} = 0, \quad p = H_p, p_s, \quad (4)$$

where $\frac{\partial \psi'}{\partial x} = v'$, $\frac{\partial \psi'}{\partial y} = -u'$, $q' = \nabla^2 \psi' + \Gamma \psi'$ is the eddy quasigeostrophic potential vorticity, $\Gamma = \frac{\partial}{\partial p} \frac{f^2}{S^2} \frac{\partial}{\partial p}$, $S^2 = -\frac{1}{\rho \theta} \frac{\partial \bar{\theta}}{\partial p}$ is the static stability, θ is potential temperature, ρ is density, f is the Coriolis parameter and H_p is the tropopause height (defined, following the World Meteorological Organization, as the lowest level where the vertical temperature gradient crosses the 2K km^{-1} value, and the average vertical gradient does not exceed 2K km^{-1} at all higher levels within 2 km^{65}). Placing a plane wave solution in Eq. (4), $\psi = \text{Re} \{ \hat{\psi}(p) e^{i(kx - \omega t)} \}$, yields an eigenvalue problem with the eigenvalues representing the growth rate of the waves^{15,44}. The mean fields (zonal wind, static stability, and tropopause height) are averaged over the mid-latitudes (30°S–60°S) and over the 1980–1999 or the 2080–2099 periods. Simplifying the mid-latitude flow to an eigenvalue problem allows us to attribute the length-scale dependent changes in the growth rate of the waves to the mean fields. This is done by re-solving Eq. (4) only keeping the mean fields constant at climatological values (i.e., averaged over the 1980–1999 period), except for one. We note that such decomposition is additive since the sum of the distinct contributions from each mean field to the growth rate changes is almost identical to the growth rate changes (compare black and green dashed lines in Supplementary Fig. 10).

DATA AVAILABILITY

The data used in the manuscript is publicly available for CMIP6, NCEP2, JRA-55 (<https://rda.ucar.edu/>), ERA5, MERRA2 (<https://gmao.gsfc.nasa.gov/reanalysis/MERRA-2/>) and CFSv2 (<https://cfs.ncep.noaa.gov/>).

CODE AVAILABILITY

The code for the normal-mode instability analysis is available at <https://doi.org/10.5281/zenodo.7948011>.

Received: 25 June 2023; Accepted: 11 November 2023;

Published online: 30 November 2023

REFERENCES

- Hartmann, D. L. *Global Physical Climatology* 2nd edn, 498 (Academic Press, 2016).
- Masson-Delmotte, V. et al. *Climate Change 2021: The Physical Science Basis. Contribution of Working Group I to the Sixth Assessment Report of the Intergovernmental Panel on Climate Change* 3–32 (Cambridge Univ. Press, 2021).

3. Schär, C. et al. The role of increasing temperature variability in European summer heatwaves. *Nature* **427**, 332–336 (2004).
4. Fischer, E. M. & Schär, C. Future changes in daily summer temperature variability: driving processes and role for temperature extremes. *Clim. Dyn.* **33**, 917–935 (2009).
5. Simolo, C. & Corti, S. Quantifying the role of variability in future intensification of heat extremes. *Nat. Commun.* **13**, 7930 (2022).
6. Kotz, M., Wenz, L., Stechemesser, A., Kalkuhl, M. & Levermann, A. Day-to-day temperature variability reduces economic growth. *Nat. Clim. Change* **11**, 319–325 (2021).
7. Tamarin-Brodsky, T., Hodges, K., Hoskins, B. J. & Shepherd, T. G. A dynamical perspective on atmospheric temperature variability and its response to climate change. *J. Clim.* **32**, 1707–1724 (2019).
8. Kotz, M., Wenz, L. & Levermann, A. Footprint of greenhouse forcing in daily temperature variability. *Proc. Natl. Acad. Sci. USA* **118**, e2103294118 (2021).
9. Schneider, T., Bischoff, T. & Plotka, H. Physics of changes in synoptic midlatitude temperature variability. *J. Clim.* **28**, 2312–2331 (2015).
10. Boer, G. J. & Shepherd, T. G. Large-scale two-dimensional turbulence in the atmosphere. *J. Atmos. Sci.* **40**, 164–184 (1983).
11. Nastrom, G. D. & Gage, K. A. A climatology of atmospheric wavenumber spectra of wind and temperature observed by commercial aircraft. *J. Atmos. Sci.* **42**, 950–960 (1985).
12. Thompson, D. W. J. & Barnes, E. A. Periodic variability in the large-scale southern hemisphere atmospheric circulation. *Science* **343**, 641–645 (2014).
13. Kidston, J., Dean, S. M., Renwick, J. A. & Vallis, G. K. A robust increase in the eddy length scale in the simulation of future climates. *Geophys. Res. Lett.* **37**, L03806 (2010).
14. Rivière, G. A dynamical interpretation of the poleward shift of the jet streams in global warming scenarios. *J. Atmos. Sci.* **68**, 1253–1272 (2011).
15. Chemke, R. & Ming, Y. Large atmospheric waves will get stronger, while small waves will get weaker by the end of the 21st century. *Geophys. Res. Lett.* **47**, e2020GL090441 (2020).
16. Sussman, H. S., Raghavendra, A., Roundy, P. E. & Dai, A. Trends in northern midlatitude atmospheric wave power from 1950 to 2099. *Clim. Dyn.* **54**, 2903–2918 (2020).
17. Graverson, R. G. & Burtu, M. Arctic amplification enhanced by latent energy transport of atmospheric planetary waves. *Q. J. R. Meteorol. Soc.* **142**, 2046–2054 (2016).
18. Mann, M. E. et al. Influence of anthropogenic climate change on planetary wave resonance and extreme weather events. *Sci. Rep.* **7**, 45242 (2017).
19. Kornhuber, K. et al. Amplified Rossby waves enhance risk of concurrent heatwaves in major breadbasket regions. *Nat. Clim. Change* **10**, 48–53 (2019).
20. Chiswell, S. M. Atmospheric wavenumber-4 driven South Pacific marine heat waves and marine cool spells. *Nat. Commun.* **12**, 4779 (2021).
21. Lembo, V. et al. Meridional-energy-transport extremes and the general circulation of Northern Hemisphere mid-latitudes: dominant weather regimes and preferred zonal wavenumbers. *Weather Clim. Dyn.* **3**, 1037–1062 (2022).
22. Di Cecco, G. J. & Gouhier, T. C. Increased spatial and temporal autocorrelation of temperature under climate change. *Sci. Rep.* **8**, 14850 (2018).
23. Li, J. & Thompson, D. W. J. Widespread changes in surface temperature persistence under climate change. *Nature* **599**, 425–430 (2021).
24. Sang, X., Yang, X.-Q., Tao, L., Fang, J. & Sun, X. Decadal changes of wintertime poleward heat and moisture transport associated with the amplified Arctic warming. *Clim. Dyn.* **58**, 137–159 (2022).
25. Pfeleiderer, P., Schleussner, C.-F., Kornhuber, K. & Coumou, D. Summer weather becomes more persistent in a 2 °C world. *Nat. Clim. Change* **9**, 666–671 (2019).
26. Vallis, G. K. *Atmospheric and Oceanic Fluid Dynamics* 770 (Cambridge University Press, 2006).
27. Xu, Z., FitzGerald, G., Guo, Y., Jalaludin, B. & Tong, S. Impact of heatwave on mortality under different heatwave definitions: a systematic review and meta-analysis. *Environ. Int.* **89**, 193–203 (2016).
28. Frölicher, T. L. & Laufkötter, C. Emerging risks from marine heat waves. *Nat. Commun.* **9**, 650 (2018).
29. Perkins-Kirkpatrick, S. E. & Gibson, P. B. Changes in regional heatwave characteristics as a function of increasing global temperature. *Sci. Rep.* **7**, 12256 (2017).
30. Frölicher, T. L., Fischer, E. M. & Gruber, N. Marine heatwaves under global warming. *Nature* **560**, 360–364 (2018).
31. Costa, N. V. & Rodrigues, R. R. Future summer marine heatwaves in the Western South Atlantic. *Geophys. Res. Lett.* **48**, e94509 (2021).
32. Perkins-Kirkpatrick, S. E. & Lewis, S. C. Increasing trends in regional heatwaves. *Nat. Commun.* **11**, 3357 (2020).
33. Perkins, S. E., Alexander, L. V. & Nairn, J. R. Increasing frequency, intensity and duration of observed global heatwaves and warm spells. *Geophys. Res. Lett.* **39**, L20714 (2012).
34. Oliver, E. C. J. et al. Longer and more frequent marine heatwaves over the past century. *Nat. Commun.* **9**, 1324 (2018).
35. Rodrigues, R. R., Taschetto, A. S., Sen Gupta, A. & Foltz, G. R. Common cause for severe droughts in South America and marine heatwaves in the South Atlantic. *Nat. Geosci.* **12**, 620–626 (2019).
36. Perkins-Kirkpatrick, S. E. et al. The role of natural variability and anthropogenic climate change in the 2017/18 Tasman Sea marine heatwave. *Bull. Am. Meteor. Soc.* **100**, S105–S110 (2019).
37. Meehl, G. A. & Tebaldi, C. More intense, more frequent, and longer lasting heat waves in the 21st century. *Science* **305**, 994–997 (2004).
38. Cowan, T. et al. More frequent, longer, and hotter heat waves for Australia in the twenty-first century. *J. Clim.* **27**, 5851–5871 (2014).
39. Feron, S. et al. Observations and projections of heat waves in South America. *Sci. Rep.* **9**, 8173 (2019).
40. Mbokodo, I., Bopape, M.-J., Chikoore, H., Engelbrecht, F. & Nethengwe, N. Heatwaves in the future warmer climate of South Africa. *Atmosphere* **11**, 712 (2020).
41. Lutsko, N. J., Baldwin, J. W. & Cronin, T. W. The impact of large-scale orography on northern hemisphere winter synoptic temperature variability. *J. Clim.* **32**, 5799–5814 (2019).
42. Patterson, M., Bracegirdle, T. & Woollings, T. Southern hemisphere atmospheric blocking in CMIP5 and future changes in the Australia-New Zealand sector. *Geophys. Res. Lett.* **46**, 9281–9290 (2019).
43. Priestley, M. D. K. et al. An overview of the extratropical storm tracks in CMIP6 historical simulations. *J. Clim.* **33**, 6315–6343 (2020).
44. Chemke, R., Ming, Y. & Yuval, J. The intensification of winter mid-latitude storm tracks in the Southern Hemisphere. *Nat. Clim. Change* **12**, 553–557 (2022).
45. Eyring, V. et al. Overview of the Coupled Model Intercomparison Project Phase 6 (CMIP6) experimental design and organization. *Geosci. Model Dev.* **9**, 1937–1958 (2016).
46. Sheshadri, A. & Plumb, R. A. Propagating annular modes: empirical orthogonal functions, principal oscillation patterns, and time scales. *J. Atmos. Sci.* **74**, 1345–1361 (2017).
47. Polvani, L. M., Waugh, D. W., Correa, G. J. P. & Son, S. W. Stratospheric ozone depletion: the main driver of twentieth-century atmospheric circulation changes in the Southern Hemisphere. *J. Clim.* **24**, 795–812 (2011).
48. Barnes, E. A., Barnes, N. W. & Polvani, L. M. Delayed Southern Hemisphere climate change induced by stratospheric ozone recovery, as projected by the CMIP5 models. *J. Clim.* **27**, 852–867 (2014).
49. Garfinkel, C. I. & Harnik, N. The non-gaussianity and spatial asymmetry of temperature extremes relative to the storm track: the role of horizontal advection. *J. Clim.* **30**, 445–464 (2017).
50. Linz, M., Chen, G. & Hu, Z. Large-scale atmospheric control on non-gaussian tails of midlatitude temperature distributions. *Geophys. Res. Lett.* **45**, 9141–9149 (2018).
51. Zhang, B., Linz, M. & Chen, G. Interpreting observed temperature probability distributions using a relationship between temperature and temperature advection. *J. Clim.* **35**, 705–724 (2022).
52. Simmons, A. J. & Hoskins, B. J. The life cycles of some nonlinear baroclinic waves. *J. Atmos. Sci.* **35**, 414–432 (1978).
53. Lorenz, E. N. Available potential energy and the maintenance of the general circulation. *Tellus* **7**, 157–167 (1955).
54. Smith, K. S. The geography of linear baroclinic instability in earth's oceans. *J. Mar. Res.* **65**, 655–683 (2007).
55. Francis, J. A. & Vavrus, S. J. Evidence linking Arctic amplification to extreme weather in mid-latitudes. *Geophys. Res. Lett.* **39**, L06801 (2012).
56. Coumou, D., Di Capua, G., Vavrus, S., Wang, L. & Wang, S. The influence of Arctic amplification on mid-latitude summer circulation. *Nat. Commun.* **9**, 2959 (2018).
57. Hersbach, H. et al. The era5 global reanalysis. *Q. J. Roy. Meteorol. Soc.* **146**, 1999–2049 (2020).
58. Kanamitsu, M. et al. Ncep-doe amip-ii reanalysis (r-2). *Bull. Am. Meteor. Soc.* **83**, 1631–1643 (2002).
59. Kobayashi, S. et al. The JRA-55 reanalysis: General specifications and basic characteristics. *J. Meteor. Soc. Japan* **93**, 5–48 (2015).
60. Gelaro, R. et al. The modern-era retrospective analysis for research and applications, version 2 (MERRA-2). *J. Clim.* **30**, 5419–5454 (2017).
61. Saha, S. et al. The NCEP climate forecast system version 2. *J. Clim.* **27**, 2185–2208 (2014).
62. Randel, W. J. & Held, I. M. Phase speed spectra of transient eddy fluxes and critical layer absorption. *J. Atmos. Sci.* **48**, 688–697 (1991).
63. Tamarin-Brodsky, T., Hodges, K., Hoskins, B. J. & Shepherd, T. G. Changes in Northern Hemisphere temperature variability shaped by regional warming patterns. *Nat. Geosci.* **13**, 414–421 (2020).
64. Perkins, S. E. & Alexander, L. V. On the measurement of heat waves. *J. Clim.* **26**, 4500–4517 (2013).
65. Birner, T. Recent widening of the tropical belt from global tropopause statistics: sensitivities. *Geophys. Res. Lett.* **115**, D23109 (2010).

ACKNOWLEDGEMENTS

I.K. is supported by the Minerva Foundation with funding from the Federal German Ministry for Education and Research. R.C. is grateful for the support of the Willner Family Leadership Institute for the Weizmann Institute of Science.

AUTHOR CONTRIBUTIONS

Both authors downloaded the data, I.K. analyzed the data, and together they discussed and wrote the paper.

COMPETING INTERESTS

The authors declare no competing interests.

ADDITIONAL INFORMATION

Supplementary information The online version contains supplementary material available at <https://doi.org/10.1038/s41612-023-00526-9>.

Correspondence and requests for materials should be addressed to Itamar Karbi.

Reprints and permission information is available at <http://www.nature.com/reprints>

Publisher's note Springer Nature remains neutral with regard to jurisdictional claims in published maps and institutional affiliations.



Open Access This article is licensed under a Creative Commons Attribution 4.0 International License, which permits use, sharing, adaptation, distribution and reproduction in any medium or format, as long as you give appropriate credit to the original author(s) and the source, provide a link to the Creative Commons license, and indicate if changes were made. The images or other third party material in this article are included in the article's Creative Commons license, unless indicated otherwise in a credit line to the material. If material is not included in the article's Creative Commons license and your intended use is not permitted by statutory regulation or exceeds the permitted use, you will need to obtain permission directly from the copyright holder. To view a copy of this license, visit <http://creativecommons.org/licenses/by/4.0/>.

© The Author(s) 2023